Photofragmentations, state interactions, and energetics of Rydberg and ion-pair states: Two-dimensional resonance enhanced multiphoton ionization of HBr via singlet-, triplet-, Ω = 0 and 2 states

Jingming Long, Helgi Rafn Hróðmarsson, Huasheng Wang, and Ágúst Kvaran

Citation: J. Chem. Phys. **136**, 214315 (2012); doi: 10.1063/1.4723810
View online: http://dx.doi.org/10.1063/1.4723810
View Table of Contents: http://jcp.aip.org/resource/1/JCPSA6/v136/i21
Published by the American Institute of Physics.

Photofragmentations, state interactions, and energetics of Rydberg and ion-pair states: Two-dimensional resonance enhanced multiphoton ionization of HBr via singlet-, triplet-, Ω = 0 and 2 states

Jingming Long, Helgi Rafn Hróðmarsson, Huasheng Wang, and Ágúst Kvaran[a)]
Science Institute, University of Iceland, Dunhagi 3, 107 Reykjavík, Iceland

(Received 15 March 2012; accepted 16 May 2012; published online 7 June 2012)

Mass spectra were recorded for one-colour resonance enhanced multiphoton ionization (REMPI) of H^iBr ($i = 79, 81$) for the two-photon resonance excitation region 79 040–80 300 cm^{-1} to obtain two-dimensional REMPI data. The data were analysed in terms of rotational line positions, intensities, and line-widths. Quantitative analysis of the data relevant to near-resonance interactions between the $F^1\Delta_2(v' = 1)$ and $V^1\Sigma^+(v' = m + 7)$ states gives interaction strengths, fractional state mixing, and parameters relevant to dissociation of the F state. Qualitative analysis further reveals the nature of state interactions between ion-pair states and the $E^1\Sigma^+$ $(v' = 1)$ and $H^1\Sigma^+(v' = 0)$ Rydberg states in terms of relative strengths and J' dependences. Large variety in line-widths, depending on electronic states and J' quantum numbers, is indicative of number of different predissociation channels. The relationship between line-widths, line-shifts, and signal intensities reveals dissociation mechanisms involving ion-pair to Rydberg state interactions prior to direct or indirect predissociations of Rydberg states. Quantum interference effects are found to be important. Moreover, observed bromine atom (2 + 1) REMPI signals support the importance of Rydberg state predissociation channels. A band system, not previously observed in REMPI, was observed and assigned to the $k^3\Pi_0(v' = 0) \leftarrow\leftarrow X$ transition with band origin 80 038 cm^{-1} and rotational parameter $B_{v'} = 7.238$ cm^{-1}.
 [http://dx.doi.org/10.1063/1.4723810]

INTRODUCTION

Photofragmentation (photodissociation and photoionization) studies of small volatile molecules is a vast research field associated with a number of intriguing and contemporary fields such as atmospheric chemistry,[1] astrochemistry,[2] and photochemical synthesis.[3] Although the literature in the field of molecular photodissociation is abundant, it is limited in terms of excitation energy ranges studied and energy- and time-resolution used in experiments. Most work deals with processes following excitations to low energy repulsive valence states. Photodissociation processes of neutrals in the less explored high energy regions largely occur via excitations to Rydberg states[4–6] followed by state interactions and curve crossings to repulsive and/or ion-pair states.[5,7]

The hydrogen halides are ideal molecules to study molecular photodissociation processes via Rydberg state excitations on a quantum energy level basis. The UV, VUV, and multiphoton excitation spectroscopy of these compounds show clearly resolved rotational structures due to excitations to Rydberg and ion-pair states.[8–11] The spectral structures are found to be rich in intensity anomalies due to state interactions and predissociation processes.[9,12–14] Since the pioneering work of Green *et al.* on HCl in 1991 (Ref. 9) and Callaghan and Gordon on HBr in 1990 (Ref. 10) a large emphasis has been on spectroscopic studies of these compounds as well as on HI to determine its high energy state properties.[11–13,15,16] More recently an increased emphasis has been on studies of state interactions and photofragmentation (photodissociation and photoionization) processes in HCl. Resonance enhanced multiphoton ionization (REMPI) techniques have proven to be powerful tools in this respect. Photofragment imaging techniques coupled with REMPI (Refs. 17 and 18) have shone light on a number of photodissociation and photoionization processes in HCl and HBr. Detailed studies of spectroscopic anomalies, such as line shifts and signal intensity irregularities, in one-colour REMPI spectra have revealed state interaction strengths as well as importance of photodissociation processes in HCl.[19–22] Theoretical *ab initio* calculations to determine excited state potential energy surfaces for HCl (Ref. 23) have proven to be very helpful for interpreting experimental data.

Most recent work, relevant to state interactions and photofragmentation processes in the hydrogen halides, in our group, has been on a number of Rydberg states and the $V^1\Sigma^+$ ion-pair state for HCl (Refs. 19–22) by the one-colour REMPI technique. Our observations can be grouped into categories depending on the strengths of Rydberg to ion-pair state interactions as follows:

a) Very weak near-resonance state interactions, distinguishable by negligible rotational line shifts but significant alterations in signal line intensities,[20] observed for triplet Rydberg states and $\Delta\Omega > 0$ state interactions.
b) Weak near-resonance state interactions, distinguishable by localized line shifts, (hence energy level shifts), as well as alterations in signal line intensities,[19,22] observed for singlet states and $\Delta\Omega > 0$ state interactions.

a)Author to whom correspondence should be addressed. Electronic mail: agust@hi.is. Telephone: +354-525-4672/+354-525-4800. Fax: +354-552-8911.

c) Medium to strong off-resonance state interactions, distinguishable by large scale line/energy level shifts, as well as alterations in signal intensities,[22,24] observed for triplet and singlet states and $\Delta\Omega = 0$ state interactions.

Whereas quite an extensive study, relevant to photofragmentations via Rydberg states of the hydrogen halides, relating to HCl has been performed, as mentioned above, limited emphasis has been placed on the heavier compounds HBr and HI. State assignments for HBr and HI resemble those for HCl. Energies for analogous states decrease with increasing molecular masses. Vibrational assignments (v') for the ion-pair states, $V^1\Sigma^+$ are uncertain and marked as $v' = m + i$, where i is integer numbers starting from $i = 1$ for the lowest energy level observed and m is an unknown integer. Based on the resemblance in the energetics of the HX's (X = Cl, Br, I) there is a reason to believe that the major photofragmentation processes in one-colour $(2 + n)$ REMPI of the hydrogen halides is similar to that summarized, pictorially, for HCl in Ref. 20. Thus the major photofragmentation processes following two-photon excitations to rovibrational (v', J') quantum levels of Rydberg (HX^{**}(Ry)) and ion-pair states (HX^{**}(V)) will typically be

(i) $HX^{**}(Ry) + h\nu \rightarrow HX^+ + e^-$;
(ii) $HX^+ + h\nu \rightarrow H^+ + X$;
(iii) $HX^{**}(V) + h\nu \rightarrow HX^+ + e^-$;
(iv) $HX^+ + h\nu \rightarrow H^+ + X$;
(v) $HX^{**}(V) + h\nu \rightarrow H + X^{**}$; $X^{**} + h\nu \rightarrow X^+ + e^-$;
(vi) $HX^{**}(V) + h\nu \rightarrow H^{**} + X$; $H^{**} + h\nu \rightarrow H^+ + e^-$;
(vii) $HX^{**}(V) + h\nu \rightarrow H^+ + X^-$;
(viii) $HX^{**}(Ry) \rightarrow H{+}X/X^*$; $X/X^* + 3h\nu \rightarrow X^+ + e^-$;
(ix) $HX^{**}(Ry) + h\nu \rightarrow H + X^{**}$; $X^{**} + h\nu \rightarrow X^+ + e^-$.

H^{**} and X^{**} are atomic Rydberg states but X and X* refer to the ground ($^2P_{3/2}$) and the spin-orbit excited ($^2P_{1/2}$) states, respectively. Channels (i) and (v–vi) typically dominate. The number of photons in the excitation processes (i–ix), however, may vary, depending on the photon energies. The initial Rydberg or ion-pair state excitations may either occur by direct two-photon excitations or via J' quantum number dependent state mixing.

In this paper, we present a REMPI work on HBr with main focus on photofragmentation and state interaction processes involving singlet Rydberg and ion-pair states. Quantitative and qualitative multiparameter analysis of line-shifts, signal intensities, and line-widths illuminate state involvements and interactions in photodissociation processes. Furthermore, observations of new spectral features will be presented.

EXPERIMENTAL

Two-dimensional (2D) REMPI data were recorded for a HBr molecular beam, created by jet expansion of a pure sample through a pulse nozzle. Apparatus used is similar to that described in Refs. 16 and 25. Excitation radiation was generated by a pulsed excimer laser-pumped dye laser systems, using a Lambda Physik COMPex205 excimer laser and a Coherent ScanMatePro dye laser. Frequency doubled radiation was focused on the molecular beam inside an ionization chamber between a repeller and an extractor plate. Ions formed by multiphoton excitations were directed into a time-of-flight tube and detected by a micro-channel plate (MCP) detector. Signals were fed into a LeCroy WaveSurfer 44MXs-A, 400 MHz storage oscilloscope and stored as a function of ion time of flights and laser radiation wavenumbers. Average signal levels were evaluated and recorded for a fixed number of laser pulses. The data were corrected for laser power and mass-calibrated to obtain ion yields as a function of mass and excitation wavenumber (2D-REMPI data). REMPI spectra for certain ions as a function of excitation wavenumber (1D-REMPI) were obtained by integrating mass signal intensities for the particular ion. Care was taken to prevent saturation effects as well as power broadening by minimising laser power. Laser calibration was based on observed $(2 + 1)$ bromine atom REMPI peaks. The accuracy of the calibration was typically found to be about ± 2.0 cm^{-1} on a two-photon wavenumber scale. Equipment condition parameters are listed in Table I.

TABLE I. Typical equipment/condition parameters for REMPI experiments.

HBr gas sample	Merck Schuchardt, Germany, Purity: 99.8%
Laser dye	C503
Frequency doubling crystal	BBO-2
Laser repetition rate	10 Hz
Dye laser bandwidth	0.095 cm^{-1}
Laser intensity used	0.1–0.3 mJ/pulse
Nozzle size	500 μm
Sample backing pressure	2.0–2.5 bars
Pressure inside ionization chamber	10^{-6} mbar
Nozzle opening time	150–200 μs
Delay time for laser excitation	450–550 μs
Excitation wavenumber step sizes	0.05–0.1 cm^{-1}
Time of flight step sizes	10 ns

RESULTS AND ANALYSIS

Spectra

2D-REMPI data corresponding to resonance transitions to the $F^1\Delta_2(v' = 1)$, $E^1\Sigma^+(v' = 1)$, $H^1\Sigma^+(v' = 0)$, $V^1\Sigma^+(v' = m + 7)$, and $V^1\Sigma^+(v' = m + 8)$ states of H^iBr ($i = 79$, 81) (see Fig. 1) in the two-photon wavenumber region 79 040–80 300 cm^{-1} were recorded, assigned, and analysed in terms of rotational line-shifts, signal intensities, and line-widths. These are hereafter named $F(1)$, $E(1)$, $H(0)$, $V(m + 7)$, and $V(m + 8)$, respectively. Figure 2 shows 1D-REMPI spectra for the H^+, $^{81}Br^+$, and $H^{81}Br^+$ ions. Within experimental error, no significant difference in rotational line positions are observed for the two isotopes, $i = 79$ and 81. Rotational line positions are listed in Table II. Several new rotational lines, not previously reported,[10] are observed. Most other peak positions agree reasonably well with those given by Callaghan and Gordon.[10] In addition to the above-mentioned resonances, weak peaks due to transitions to a Rydberg state, previously unobserved in REMPI, are observed in the region 80 028–80 040 cm^{-1} (see Fig. 2 and Table II). Furthermore, three Br atomic

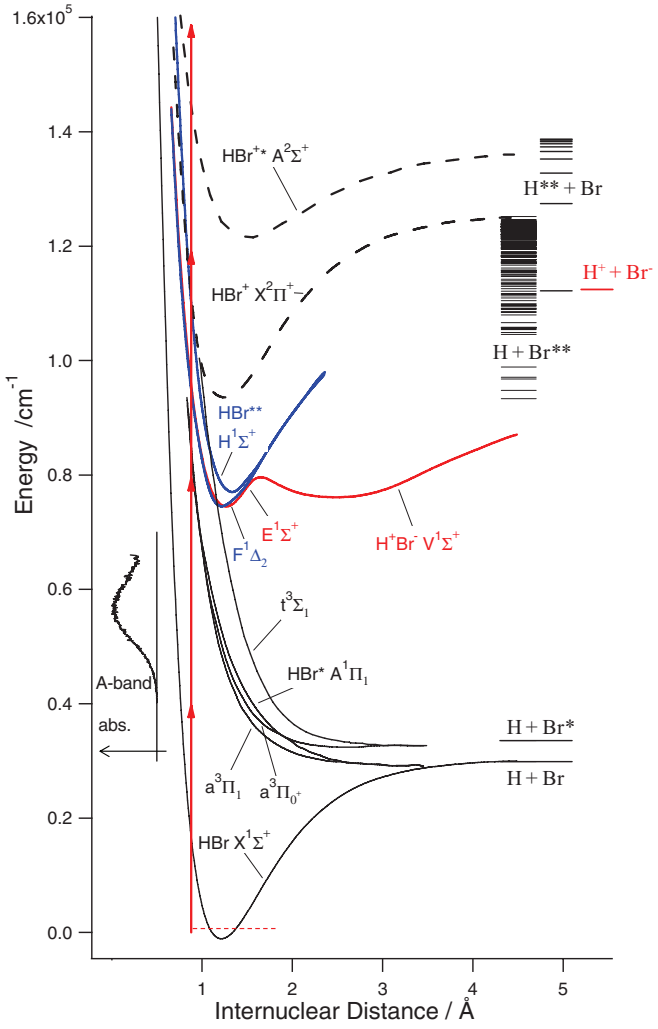

FIG. 1. HBr energetics. Potential energy curves, asymptotic energies (right), photon excitations (red arrows; left) corresponding to two-photon resonance excitation to the $F^1\Delta_2(v' = 1)$ state and relative absorption intensity of the *A*-band (Ref. 33) (tilted to the left). Potential curves other than the repulsive states are derived from Fig. 1 in Ref. 18. Repulsive potentials (*A*, *t* and the *a* states) are derived from Fig. 1 in Ref. 34. Threshold energies are derived from atom energy levels.[35]

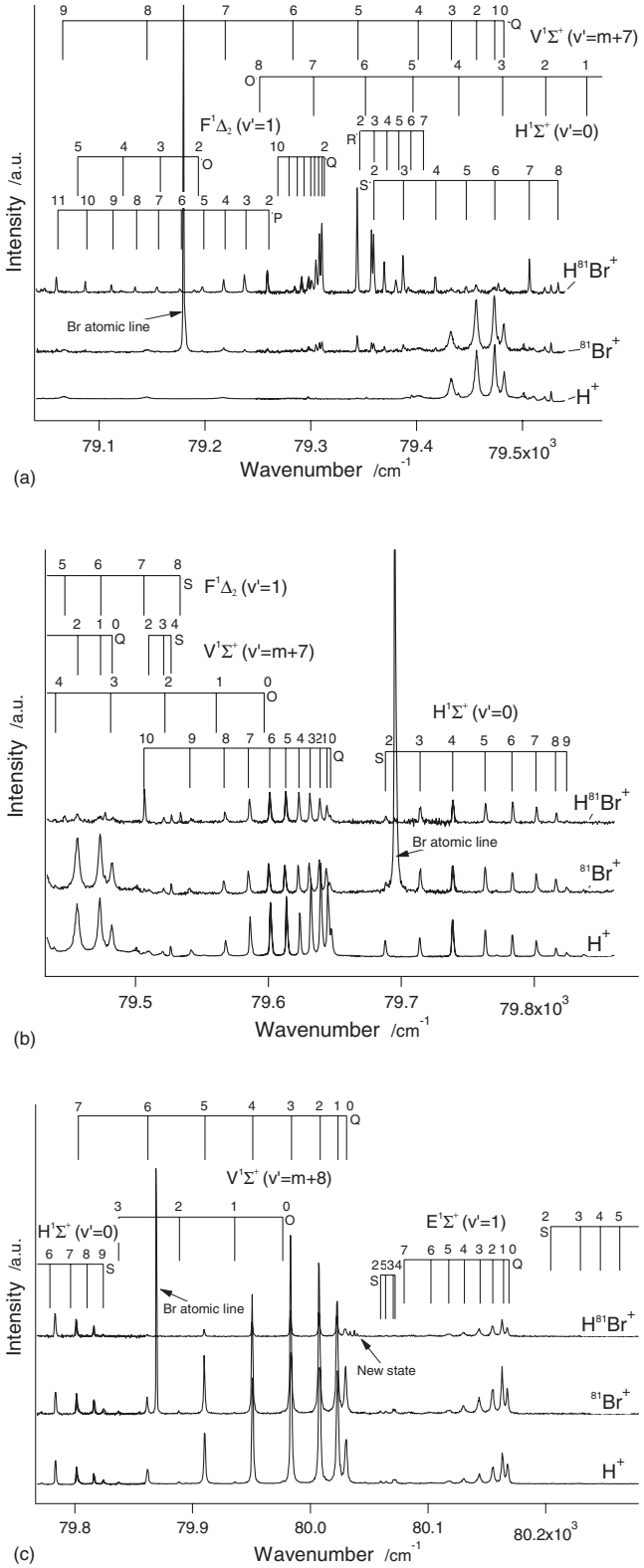

FIG. 2. 1D-REMPI spectra for H^+, $^{81}Br^+$, and $H^{81}Br^+$ and J' assignments for rotational peaks corresponding to two-photon resonance excitations to the $F^1\Delta_2(v' = 1)$, $V^1\Sigma^+(v' = m + 7)$, $H^1\Sigma^+$ $(v' = 0)$, $V^1\Sigma^+(v' = m + 8)$, and $E^1\Sigma^+$ $(v' = 1)$ states. New, previously unreported spectrum in REMPI, assigned to two-photon resonance transition to the $k^3\Pi_0(v' = 0)$ state is marked in figure (d). Three atomic lines due to (2 + 1) REMPI of Br are also marked (see Table VI).

(2 + 1) REMPI resonances, due to transitions from ground state Br($^2P_{3/2}$) to the excited states $^4S_{3/2}$ (79 178 cm^{-1}), $^2P_{3/2}$ (79 696 cm^{-1}), and $^2P_{1/2}$ (79 868 cm^{-1}), were identified in the spectral region.

Analysis of the spectrum near 80 040 cm^{-1}, based on the assumption that the peaks are *Q* lines, gave rotational constants $B_{v'} = 7.238 \pm 0.070$ cm^{-1} and $D_{v'} = -0.016 \pm 0.005$ cm^{-1} and band origin value of 80 038 ± 2 cm^{-1} for the Rydberg state. Based on comparison with absorption data given by Ginter *et al.*,[26] the state of concern is assigned $k^3\Pi_0$ $(v' = 0)$.

Energetics and line-shifts vs. state interactions

Rotational level energies for all five states were derived from the line positions (Table II) and the rotational level energies of the H^{81}Br ground state[27] (see Fig. 3). To a first approximation an unperturbed state will show linear behaviour

TABLE II. Rotational lines for H^{i}Br (i = 79, 81), due to two-photon resonance transitions to the $V^1\Sigma^+(v' = m + 7)$, $V^1\Sigma^+(v' = m + 8)$, $E^1\Sigma^+(v' = 1)$, $F^1\Delta_2(v' = 1)$, $H^1\Sigma^+(v' = 0)$ and "New" ($k^3\Pi_0(v' = 0)$) states (see text).

	$V(m+7)$		$V(m+8)$			E(1)				
J'	Q	S	O	Q	S	Q	S			
0	79 481.3		79 975.5	80 029.0		80 166.3				
1	79 472.5		79 934.8	80 021.8		80 162.0				
2	79 455.4	79 508.8	79 887.3	80 006.6	80 058.5	80 153.8	80 203.1			
3	79 431.7	79 520.0	79 836.0	79 982.4	80 069.3	80 142.2	80 228.3			
4	79 399.6	79 525.6[a]		79 949.7	80 070.9	80 129.1	80 245.2			
5	79 343.4[a]			79 909.0	80 063.3	80 116.4	80 261.6			
6	79 282.1[a]			79 860.5	80 045.5	80 101.2[a]	80 278.0[a]			
7	79 218.1[a]			79 801.8[a]		80 083.5[a]	80 296.3[a]			
8	79 144.2[a]						80 314.6[a]			
9	79 064.5[a]									

	$F(1)$					$H(0)$			New
J'	O	P	Q	R	S	O	Q	S	Q
0						79 595.6	79 645.6		80 039.8[a]
1						79 559.5	79 642.9		80 037.5[a]
2	79 191.2	79 258.2	79 309.6	79 343.0	79 358.6	79 520.9	79 637.7	79 686.8	80 033.8[a]
3	79 155.2	79 236.6	79 307.3	79 356.6	79 386.5	79 480.1	79 630.2	79 712.9	80 028.8[a]
4	79 120.1	79 216.9	79 304.1	79 368.6	79 417.0	79 438.6	79 621.8	79 737.3	
5	79 077.1[a]	79 196.6	79 300.2	79 379.7	79 445.8	79 395.5	79 611.8	79 761.7	
6	79 047.0	79 175.5	79 296.7	79 391.2	79 472.7	79 350.5	79 599.8	79 782.0	
7		79 153.9	79 290.4	79 403.1	79 505.2[a]	79 301.6[a]	79 583.7	79 800.0	
8		79 133.2[a]	79 283.9		79 532.4[a]	79 250.6[a]	79 565.4	79 814.8	
9		79 111.0[a]	79 276.1				79 539.7	79 823.2[a]	
10		79 086.2[a]	79 265.7				79 505.2[a]		
11		79 058.9[a]							

[a]New, previously unobserved peaks in REMPI.

for the energy spacing between neighbour energy levels, $\Delta E_{J',J'-1}$ $(= E(J') - E(J' - 1))$ as a function of J' with a slope value $2B_{v'}$, where $B_{v'}$ is the v'-dependent rotational constant. Irregular, nonlinear, shape of $\Delta E_{J',J'-1}$ vs J' plots is a clear indication of perturbation effects due to state interactions (see Fig. 4) showing as level-to-level repulsions between levels with same J' numbers.[12,28] The shift of an energy level of a perturbed state (1) $(\Delta E_{J'}(1) = E_{J'}(1) - E^0_{J'}(1)$, where $E^0_{J'}(1)$ is the zero order energy for the unperturbed state) depends on the interaction strength (W_{12}) between that state (1) and the perturbing state (2) and the observed energy level difference, between the two states, for same J' (i.e., $\Delta E_{J'}(1, 2) = E_{J'}(1) - E_{J'}(2)$),

$$\Delta E_{J'}(1) = \frac{1}{2}\left(\Delta E_{J'}(1,2) - \sqrt{(\Delta E_{J'}(1,2))^2 - 4\,|W_{12}|^2}\right). \tag{1a}$$

Equation (1a) is derived from the classical expression given by Herzberg[28] for energies in case of level-to-level interactions,

$$E_{J'}(i) = \frac{1}{2}\left(E^0_{J'}(1) + E^0_{J'}(2)\right) \pm \frac{1}{2}\sqrt{4\,|W_{12}|^2 + (\Delta E^0_{J'}(1,2))^2}; \quad i = 1, 2$$
$$\Delta E^0_{J'}(1,2) = E^0_{J'}(1) - E^0_{J'}(2). \tag{1b}$$

Small, but significant, positive deviation of the $\Delta E_{J',J'-1}$ value from linearity for $J' = 6$ (slight negative deviation for $J' = 7$) in $F(1)$ is an indication of near-resonance interactions between $F(1)$ and $V(m + 7)$ (Ref. 13) (see Fig. 3(a)). Strictly, interaction between the $F^1\Delta_2$ and $V^1\Sigma^+(0^+)$ states violates the selection rule $\Delta\Omega = 0, \pm 1$. Most probably, however, the F-state is a mixed state analogous to HCl, where the F-state wave function is believed to be a linear combination of Ω = 1, 2, and 3 components, and F to V perturbations observed therefore due to heterogeneous $(\Delta\Omega = 1)$.[19,29] The larger irregularities in energy levels, observed for the $V(m$ + 7) state, however, (Fig. 4(a)) indicates further involvement of larger homogeneous $(\Delta\Omega = 0)$ state interactions with $\Omega = 0$ states, of which interaction with the $E(1)$ state, slightly higher in energy, will dominate. Involvement of the closer in energy $H(0)$ state, however, will also be affective. A positive deviation in $\Delta E_{J',J'-1}$ values vs. J' observed for $E(1)$ (see Fig. 4(a)) acts in accordance with a large negative deviation observed for $V(\mathrm{m} + 7)$ near $J' = 4$–6. The $E(1)$ state does, however, "experience" still stronger interactions from the "closer in energy" $V(m + 8)$ and $V(m + 9)$ states which all together will affect the observed irregularities in $\Delta E_{J',J'+1}$ vs. J' for $E(1)$. Whereas almost a linear behaviour of $\Delta E_{J',J'-1}$ vs. J' is observed for $H(0)$ (Fig. 4(b)), in the low J' region, large negative deviation is observed for high J' $(J' > 6)$. The major perturbation effects on $H(0)$ will be due to interactions

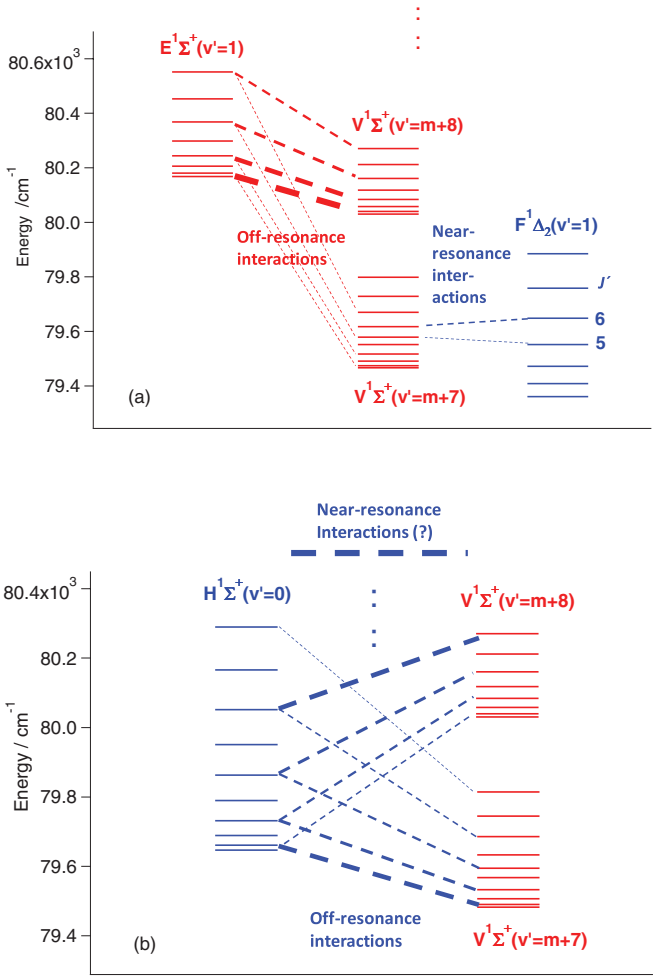

FIG. 3. Rotational energy levels, derived from observed REMPI rotational peaks for the $F^1\Delta_2(v' = 1)$(a), $V^1\Sigma^+(v' = m{+}7)$((a) and (b)), $H^1\Sigma^+(v' = 0)$(b), $V^1\Sigma^+(v' = m + 8)$((a) and (b)) and $E\,^1\Sigma^+$ $(v' = 1)$(a) states. Observed level-to-level near-resonance interactions between $F(1)$ and $V(m + 7)$ and off-resonance interactions between the $V(m + 7)$ and $V(m + 8)$ ion-pair states and the $E(1)$ and $H(0)$ Rydberg states are indicated by broken lines. Strength and alterations in state mixings are indicated, roughly, by varying thickness of broken lines.

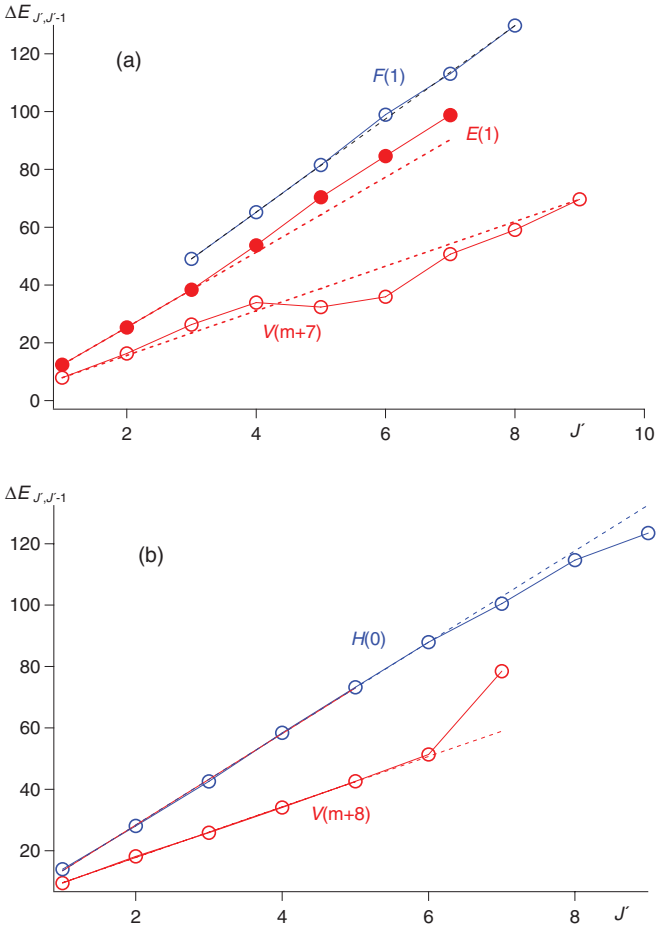

FIG. 4. H^iBr: Spacings between rotational levels ($\Delta E_{J',\,J'-1}$) as a function of J' for $F^1\Delta_2(v' = 1)$(a), $E^1\Sigma^+(v' = 1)$(a), $V^1\Sigma^+(v' = m + 7)$(a), $H^1\Sigma^+(v' = 0)$(b), and $V^1\Sigma^+(v' = m + 8)$(b). Dots connected by solid lines are derived from Q rotational lines. Broken lines are line fits for, $J' = 3$–5 and 8 values for $F(1)$, $J' = 1$–3 values for $E(1)$, $J' = 1$–6 values for $H(0)$, and $J' = 1$–5 values for $V(m + 8)$. The broken line for $V(m + 7)$ joins the dots for $J' = 1$ and 9 to guide the eye.

with the V state. These observations, therefore, suggest that overall effects due to level-to-level interactions with the $V(m + 7)$ and $V(m + 8)$ states "cancel", such that a decreasing level repulsions with J' by $V(m + 7)$ matches an increasing repulsions with J' by $V(m + 8)$ (Fig. 3(b)), resulting in an effective lowering in the slope, hence the rotational constant. The growing negative deviation for high J', on the other hand, is due to increasing near-resonance-interactions with $V(m + 8)$ also observed as positive deviation in the $\Delta E_{J',\,J'-1}$ vs. J' plot for $V(m + 8)$.

Assuming only level-to-level interaction with $V(m + 7)$ to be responsible for the energy deviations observed in $F(1)$ (Fig. 4(a)), the interaction strength for $J' = 6$ could be evaluated from Eq. (1) as $W_{12} = 4.4 \pm 0.4\ \mathrm{cm}^{-1}$. Furthermore, by assuming the heterogeneous interaction to change with J' as

$$W_{12} = W'_{12}(J'(J' + 1))^{1/2}. \tag{2}$$

$W'_{12} = 0.68 \pm 0.07\ \mathrm{cm}^{-1}$ was derived and W_{12} values for J' = 2–7 evaluated (Table III). The fractional contributions to the state mixing, c_1^2 and c_2^2, for the states 1(F(1)) and 2(V($m + 7$)) respectively can now easily be derived from

$$c_1^2 = \frac{1}{2} + \frac{\sqrt{(\Delta E_{J'}(1,2))^2 - 4\,|W_{12}|^2}}{2\,|\Delta E_{J'}(1,2)|}; \quad c_2^2 = 1 - c_1^2 \tag{3}$$

(see Table III).

Signal intensities vs. state interactions

Rotational lines were fitted by Lorentzian functions to obtain integrated intensities as well as line-widths. $^iBr^+$ signal intensities relative to H^iBr^+ signal intensities ($I(^iBr^+)/I(H^iBr^+)$) as a function of J', for the Rydberg state spectra (see Fig. 5) show certain resemblance to analogous plots of $I(^iCl^+)/I(H^iCl^+)$ for H^iCl (Refs. 19–22) where an increase in the ratio has been shown to indicate an accession of state mixing and stronger interaction with the $V^1\Sigma^+$ ion-pair state. Thus the plot of the Q line intensity ratios for the $F(1)$ state shows a weak but significant increase for $J' = 6$ (Fig. 5(a)) corresponding to the near-resonance

TABLE III. Parameters derived from line-shift and intensity-ratio ($I(^iBr^+)/I(H^iBr^+)$) analysis of the $F(1) \leftarrow\leftarrow X$ system (see Figs. 4(a), 6(a), and 6(b))

J'	$\Delta E = E(F(1) - E(V(m+7)))$	W_{12}	$c_1{}^2$	$c_2{}^2$
2	−145.9	1.67	1.00	0.000
3	−124.4	2.36	1.00	0.000
4	−95.5	3.046	1.00	0.000
5	−43.2	3.73	0.993	0.007
6	14.6	4.41	0.898	0.102
7	72.3	5.09	0.995	0.005
W'_{12}	0.68 ± 0.07 cm^{-1}			
γ (β_1/α_2)	0.11			
α (α_2/α_1)	1.3			
$\alpha\gamma$ (β_1/α_1)	0.14			

interaction with $V(m+7)$ (see Fig. 3(a)). This near-resonance effect also displays itself as alterations in absolute ion signals. Thus the P line series for H^iBr^+ displays minimum for $J' \sim 6$ (see Fig. 2(a)) and the $J' = 6$ peak for H^+ in the Q line series exhibits enlargement. The intensity ratios ($I(^iBr^+)/I(H^iBr^+)$) for the $E(1)$ state gradually decrease with J' (Fig. 5(c)), indicating less off-resonance interactions with $V(m+8)$ as the spacing between the levels ($\Delta E_{J'}(E(1),V(m+8))$) increases with equal J' (Fig. 3(a)). There is, however, a slight indication of an enhanced ratio near $J' = 6$ (Fig. 5(c)). The intensity ratios for $H(0)$ show clear effect of "double" state interactions, showing decreasing values with J' for low J' (for $J' > 0$) but increasing values with J' for high J', with minimum at $J' \sim 5$ (Fig. 5(d)). This is due to a decreasing interaction with $V(m+7)$ but increasing interaction with $V(m+8)$ as a function of J' and the $\Delta E_{J'}(H(0),V)$'s increase and decrease for $V(m+7)$ and $V(m+8)$ respectively (Fig. 3(b)).

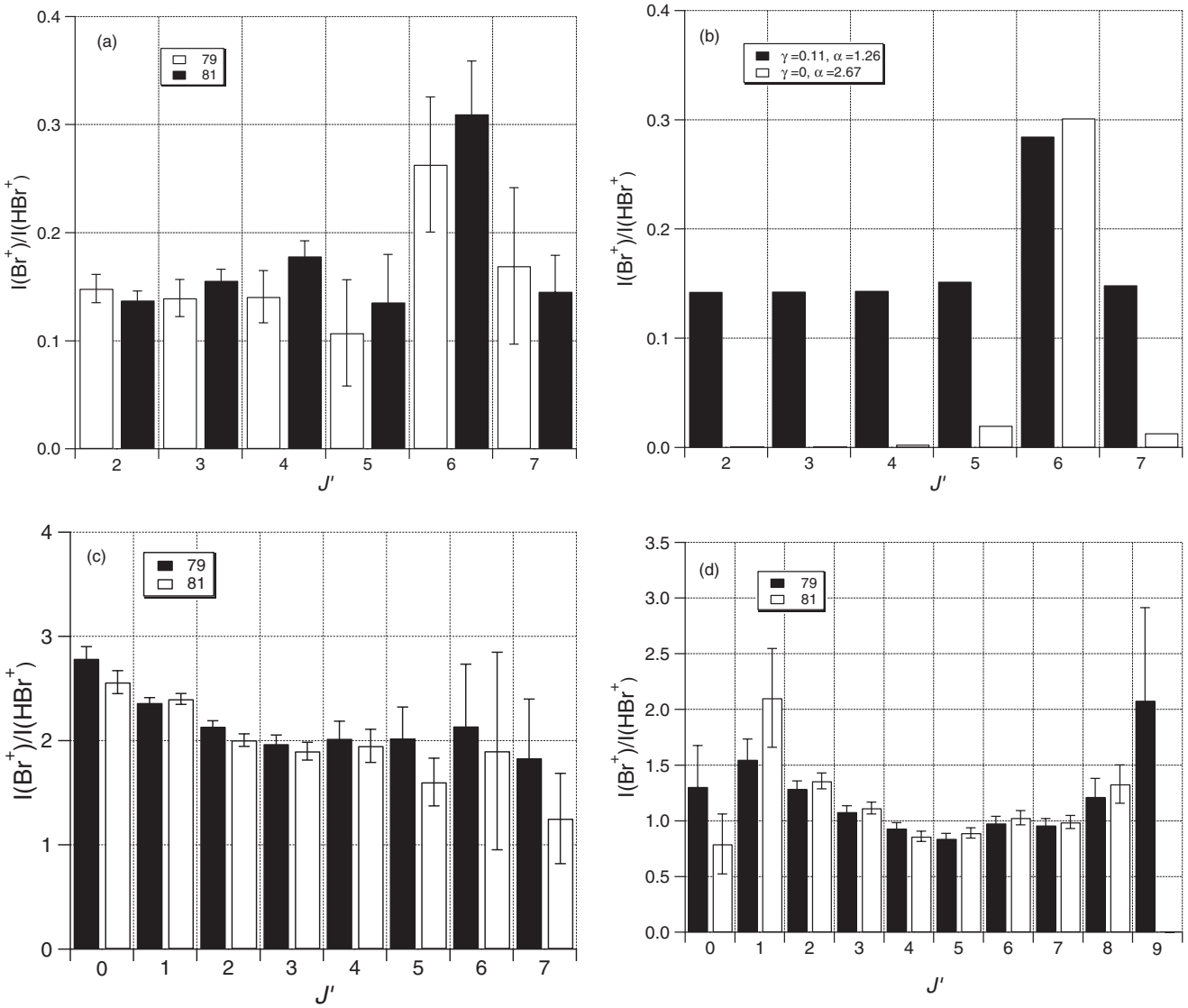

FIG. 5. Relative ion signal intensities, $I(^iBr^+)/I(H^iBr^+)$ (i = 79, 81) vs. J' derived from Q rotational lines of REMPI spectra due to two-photon resonance transitions to the Rydberg states $F(1)$ (a), $E(1)$(c), and $H(0)$(d). (b) shows simulation for (a), assuming J' level-to-level interactions between the $F(1)$ and $V(m+7)$ states (black columns) for $W'_{12} = 0.68$ cm^{-1}, $\alpha = 1.26$, and $\gamma = 0.11$ as well as calculated ratios for same W'_{12}, $\alpha = 2.67$, and $\gamma = 0$ (white columns) (see text).

By analogy with the observations for HCl, as mentioned before, in case of level-to-level interactions between two states (1) (Rydberg state) and (2) (ion-pair state), $I(^iBr^+)/I(H^iBr^+)$ can be expressed as

$$\frac{I(^iBr^+)}{I(H^iBr^+)} = \frac{\alpha\left[\gamma + c_2^2(1-\gamma)\right]}{\left(1-c_2^2\right)}, \tag{4}$$

where

$$I(^iBr^+) = \alpha_2 c_2^2 + \beta_1 c_1^2; \quad I(H^iBr^+) = \alpha_1 c_1^2 + \beta_2 c_2^2$$
$$\alpha = \alpha_2/\alpha_1; \quad \gamma = \beta_1/\alpha_2; \quad \alpha\gamma = \beta_1/\alpha_1$$

α_i and β_i (i = 1, 2) are ionization rate coefficients for the excited molecular states (1) and (2). By least square fitting the expression on the right side of Eq. (3) to the experimental intensity ratios, as a function of J', derived from the $F(1)$ state spectra (Fig. 5(a)) using the W_{12} values obtained from the line shift analysis mentioned above and the energy level differences ($\Delta E_J(1, 2)$; Table III), $\alpha = 1.26$, $\gamma = 0.11$, and $\alpha\gamma = 0.14$ values were obtained (see Fig. 5(b)). γ, hence $\alpha\gamma$, are measures of $^iBr^+$ ion formations via dissociation of the Rydberg state, relative to that of the formations of $^iBr^+$ via exciations of the ion-pair state and relative to that of the formations of H^iBr^+ via excitation of the Rydberg state respectively. Whereas no γ and $\alpha\gamma$ values have been reported for HBr before, γ derived for HCl are found to be in the range γ = 0–0.03 (Refs. 20 and 22) depending on Rydberg states. The significance of the nonzero and relatively high γ value of 0.11, derived here, can be deduced from the dramatic effect of replacing it with $\gamma = 0$ in the calculations (see Fig. 5(b)). This suggests that predissociation of the $F(1)$ state to form H + Br/Br* is important.

Line-widths and fragmentations vs. state interactions

Rotational line-widths vary a lot depending on the resonance excited states and rotational levels as seen in Fig. 2, indicating a large variation in lifetimes of states. Figure 6 shows rotational line-widths (Γ) as a function of J'. Lower limit lifetimes (τ) derived from[6,30]

$$\tau(\text{ps}) = 5.3/\Gamma(\text{cm}^{-1}) \tag{5}$$

are listed in Table IV. The line-widths for the Q lines of the $H(0)$ spectrum (Fig. 6(f)) show close correspondence to the intensity ratios as a function of J' (Fig. 5(d)) previously explained to reflect interactions with both $V(m + 7)$ and $V(m + 8)$. For $F(1)$, line-widths as a function of J', derived from the line series P, Q, R, and S all show small but significant maxima, hence lifetime minima, near $J' = 5$ (see Figs. 6(a)–6(c)). The $V(m + 7)$ state, showing very broad peaks, also exhibits maximum bandwidth (minimum lifetime) for $J' \sim 5$–6 and much shorter lifetimes than $F(1)$ (Fig. 6(d)). Due to very weak intensity and breadth of the $V(m + 7)$, Q line, $J' = 5$ peak line-width could not be determined. Line-widths for the $E(1)$ state are in range between those for $F(1)$ and $V(m + 7)$, also reaching maximum for $J' = 5$ (Fig. 6(e)). This further indicates close interactions between the states involved in agreement with previous interpretations of line shifts and intensity ratios. There are, however, considerable, important correlation differences between the various observation parameters for $F(1)$ and $E(1)$. The maximum line-shifts and $I(^iBr^+)/I(H^iBr^+)$ intensity ratios, for $F(1)$, are observed for $J' = 6$ whereas the maximum bandwidths (minimum lifetime) are found for $J' = 5$. Furthermore, line-widths of the Q lines for $E(1)$ (Fig. 6(e)) show significantly different behaviour with J' compared to that of the intensity ratios (Fig. 5(c)). The explanation lies in the fundamental differences in the observation parameters. Line-widths, hence lifetimes, are primarily determined by the rates of crossing from the bound excited states to continua (i.e., predissociation), whereas the line-shifts and intensity irregularities are primarily indicative of bound-to-bound state interactions. However, predissociation can occur via interacting gateway states, thus making the lifetimes state interaction dependent. Figures 3(a) and 3(b) summarize the major level-to-level state interactions of concern. The large average internuclear distance of the V state makes crossing to repulsive states, for which the repulsive walls are at much shorter internuclear distances (see Fig. 1), highly improbable. The Rydberg states, on the other hand, are either in close vicinity of or crossed by repulsive states to make predissociation processes more probable. Therefore, we believe that the short lifetimes observed, are mainly due to predissociation of Rydberg states, either directly or via Rydberg gateway states analogous to that assumed to hold for HCl.[20,22,31] Hence, the particularly short lifetimes, observed for the $V(m + 7)$ state are due to predissociation processes following crossings from $V(m + 7)$ to Rydberg states such as the $E(1)$, $F(1)$, and $H(0)$ states. This is demonstrated schematically in Fig. 7 for the $V(m + 7)$, $E(1)$, and $F(1)$ states. Based on a coupling scheme given by Alexander *et al.*[31] a summary of state couplings due to spin-orbit-(SO) and rotational-(JL and JS) interactions between relevant states are shown in Table V. SO couplings, generally, are the strongest interactions with coupling strengths independent of rotational energies, whereas weaker rotational interactions will increase with rotational energies. It should be noted, however, that in both cases the bound-to-bound state mixing (c_i^2) will depend on the spacing between the rotational levels with same rotational quantum numbers (ΔE_J) (Eq. (3)) making the effective interaction in both

TABLE IV. (Lower limit) lifetimes (ps) of rotational states (J') derived from REMPI spectra line-widths (see text). The values were derived from Q lines of H^iBr^+ (i = 79, 81) signals for $E(1)$, $F(1)$, and $H(0)$ but from Q lines of H^+ signals for $V(m + 7)$.

J'	$V(m+7)$	$E(0)$	$F(1)$	$H(0)$
0	1.69 ± 0.34	2.29 ± 0.07		1.96 ± 0.38
1	1.64 ± 0.28	2.50 ± 0.04		3.86 ± 0.38
2	1.41 ± 0.07	1.86 ± 0.04	3.96 ± 0.05	3.65 ± 0.15
3	1.16 ± 0.12	1.39 ± 0.04	4.01 ± 0.07	3.78 ± 0.13
4	0.65 ± 0.06	1.24 ± 0.07	3.10 ± 0.08	4.38 ± 0.15
5		1.08 ± 0.11	2.37 ± 0.16	4.52 ± 0.16
6	0.48 ± 0.13	1.36 ± 0.34	3.23 ± 0.22	4.10 ± 0.17
7	0.59 ± 0.03	1.46 ± 0.63	3.84 ± 0.27	3.63 ± 0.15
8	0.86 ± 0.05		4.05 ± 0.74	2.99 ± 0.31
9	1.03 ± 0.07		3.44 ± 2.23	3.21 ± 1.46

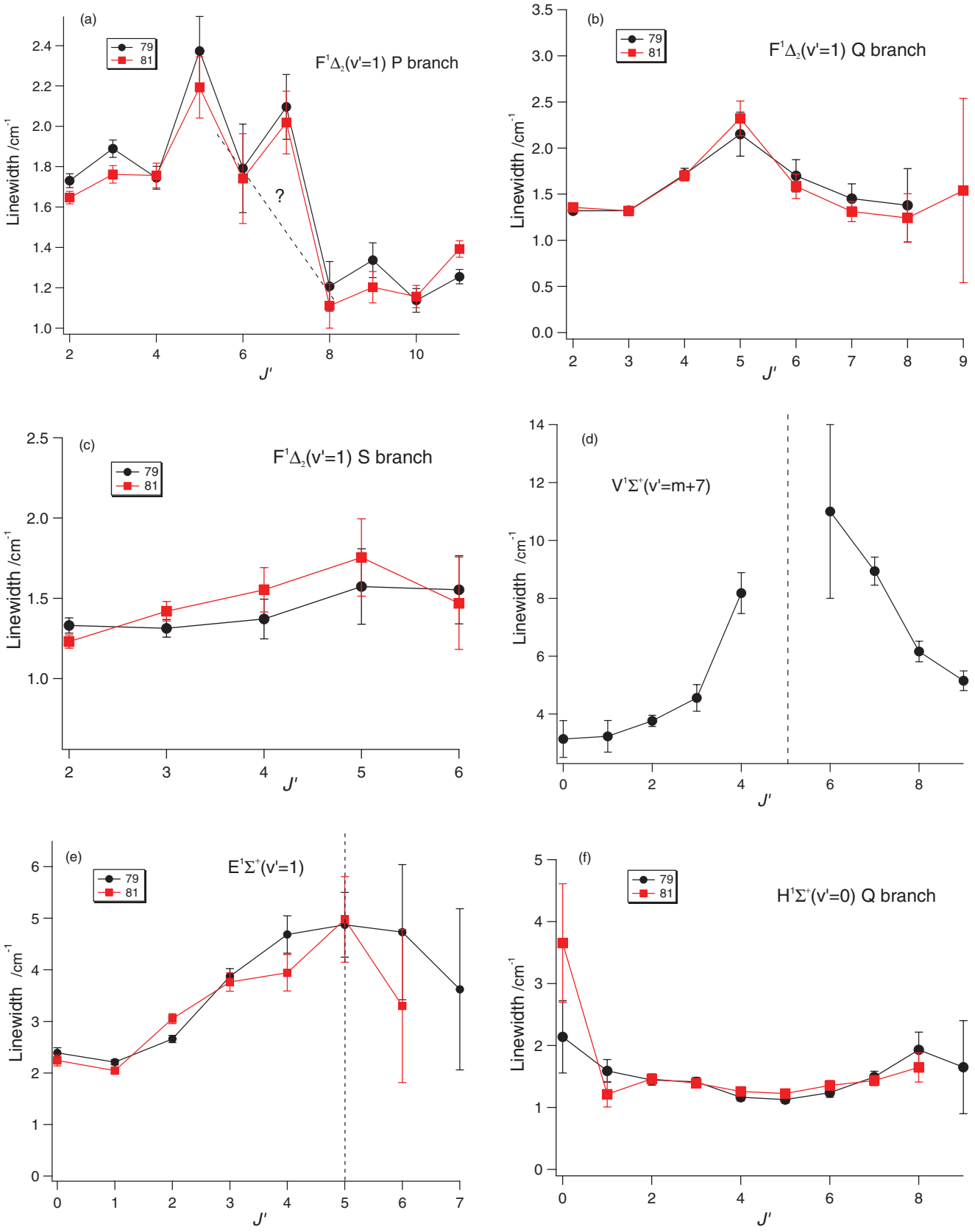

FIG. 6. Rotational line-widths vs. J' derived from REMPI spectra for (a) $F(1)$, P lines, H^iBr^+ (i = 79, 81), (b) $F(1)$, Q lines, H^iBr^+, (c) $F(1)$, S lines, H^iBr^+, (d) $V(m + 7)$, Q lines, H^+, (e) $E(1)$, Q lines, H^iBr^+, (f) $H(0)$, Q lines, H^iBr^+. The line-width derived for $F(1)$, P line, $J' = 7$ (a) is overestimated due to overlap of peaks $P(J' = 7)$ and $O(J' = 4)$ (see Fig. 2(a)). Due to very weak intensity and breadth of the $V(m + 7)$, Q line, $J' = 5$ peak line-width could not be determined (d).

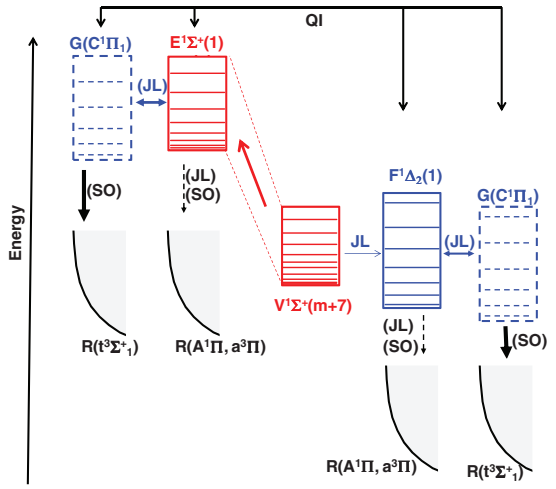

FIG. 7. Semischematic figure, showing the H^{i}Br energetics, state interactions, and transfers of relevance. Rotational and spin-orbit couplings are marked *JL* and *SO,* respectively. States marked *G* and *R* are gateway and repulsive states, respectively. States and couplings inside brackets are example cases believed to be of importance. Relative importance of couplings and transfers are indicated by different boldness of arrows. Quantum interference effects between states are indicated by arrows marked *QI*.

cases rotational energy dependent. Furthermore, interaction strengths will depend on Franck-Condon-overlaps, favouring interactions between Rydberg states and repulsive states close to curve-crossings. Involvements of the repulsive states $t^3\Sigma$ (see Fig. 1) are therefore expected to be important in predissociation processes. Considering all these factors, the $E(1)$ and $F(1)$ states (hence the mixed $V(m+7)$ state) could be largely affected by *SO* couplings of the $C^1\Pi_1$-gateway state with the repulsive $t^3\Sigma^+{}_1$ state following rotational (*JL*) couplings with the *C*-state. Direct predissociation of the $E(1)$ and $F(1)$ states by the *A* and the *a* states will also be involved but to a less extent (see Fig. 7). Furthermore the *C* to *F* state mixing will be important in enhancing the rotational/heterogeneous ($\Delta\Omega = 1$) coupling between the $V(m+7)$ and the $F(1)$ state. The bound-bound rotational couplings (*JL*) will have the greatest effect on the rotational

TABLE V. State couplings based on correlation diagrams from Ref. 31. Spin-orbit couplings are marked *SO*. Rotational couplings, *L* uncoupled and *S*-uncoupled, are marked *JL* and *JS*, respectively.

State interactions		Bound states					
		E, H, V	*F*	*C,D* $^1\Pi_1$	$b^3\Pi_0$	$b^3\Pi_2$	$g^3\Sigma_0^-$
Continuum states	$A^1\Pi_1$	*JL*	*JL*				
	$a^3\Pi_2$		*SO*				
	$a^3\Pi_1$			*SO*	*JS*	*JS*	*JL*
	$a^3\Pi_0{}^-$(e)	*SO*					*SO*
	$t^3\Sigma_1{}^+$			*SO*		*JL*	
	$t^3\Sigma_0{}^+$(f)				*SO*		
Bound states	*C,D* $^1\Pi_1$		*JL*				
	$b^3\Pi_0$	*SO*					
	$b^3\Pi_2$		*SO*				
	$g^3\Sigma_0^-$	*SO*					

energy dependence of the line-width/lifetime. The close correlation observed between the $E(1)$ and $F(1)$ states, in terms of the J'-dependent line-widths, showing as maxima for the same J' ($J' \sim 5$) strongly suggests that quantum interference (*QI*; Fig. 7) effects apply, involving the Rydberg states $E(1)$, $F(1)$, and $C^1\Pi$. The slight increases observed in the intensity ratios ($I(^i\mathrm{Br}^+)/I(\mathrm{H}^i\mathrm{Br}^+)$) both for the $E(1)$ and $F(1)$ states at $J' = 6$ (Figs. 5(a) and 6(c)) further demonstrate this.

Considering interaction schemes such as the one presented in Fig. 7, an approximation expression, relating lifetimes of the $V(m+7)$, $E(1)$, $F(1)$, and $H(1)$ states, can be derived. The basic idea is that the lifetime of $V(m+7)$ is determined by the lifetimes of the Rydberg states, which $V(m+7)$ couples with. Assuming the rate of dissociation of $V(m+7)$, due to a coupling with a Rydberg state, to be proportional to the rate of dissociation of that Rydberg state and the state mixing the following approximation expression, relating rate coefficients ($1/\tau_i$), can be written,

$$\frac{1}{\tau_{V7}} = f_{E1}\frac{1}{\tau_{E1}} + f_{F1}\frac{1}{\tau_{F1}} + f_{H0}\frac{1}{\tau_{H0}} + f_{\mathrm{other}}\frac{1}{\tau_{\mathrm{other}}}, \qquad (6)$$

where τ_i ($i = V7, E1, F1, H0$, other) are the lifetimes of the $V(m+7)$, $E(1)$, $F(1)$, $H(0)$, and other states, respectively. The f_i's are proportionally coefficients, depending on coupling rates. Since the rate of dissociation of $V(m+7)$, via coupling with a particular Rydberg state, cannot exceed the rate of dissociation of that Rydberg state the corresponding f_i-factor cannot be larger than one, hence $0 \le f_i \le 1$. Consistent variations in the bandwidths with J', observed for all measurements in ranges larger than our detection limit of about 0.3 cm^{-1}, make us believe that the lifetime values for the $V(m+7)$, $E(1)$, $F(1)$, and $H(0)$ states (Table IV) are reasonable estimates for the absolute values within uncertainty limits. There is a reason to expect that the states $E(1)$, $F(1)$, and $H(0)$ contribute the most to the observed dissociation rate of $V(m+7)$ and that contributions from other states are less or minor in the case of the shortest lifetimes. For $J' = 4$, 6, and 7 the rate of dissociation for $V(m+7)$ ($1/\tau_{V7}$) derived from the lifetimes in Table IV is in fact found to be close to or only slightly higher than the sum of the dissociation rates of the $E(1)$, $F(1)$, and $H(0)$ ($1/\tau_{E1} + 1/\tau_{F1} + 1/\tau_{H0}$), within uncertainty limits. This suggests that the corresponding f_i factors are close to unity. Analogous comparison could not be made for $J' = 5$, since its bandwidth for $V(m+7)$ could not be determined (see figure caption 6(d)). Assuming $fi = 1$ ($i = E1, F1, H0$) and $f_{\mathrm{other}} = 0$ the lifetime for $J' = 5$ is estimated to be about 0.64 ps, hence the line-width about 8.3 cm^{-1}.

Bromine atomic lines

Generally it is believed that Br atomic lines observed in REMPI of HBr are primarily due to REMPI of Br atoms following one-photon photodissociation via the repulsive state $A^1\Pi$.[18] Considering the number of evidences for photofragmentations via Rydberg states, mentioned above, these must also be, partly or largely, due to REMPI of Br atoms formed by predissociations of Rydberg states following two-photon excitations. Thus it will resemble

TABLE VI. (2 + 1) REMPI bromine atomic lines and closest H^{i}Br rotational lines.

Bromine atomic lines			H^{i}Br rotational peaks		
Two-photon transitions	ν (cm^{-1}), our values	Relative intensity	Rotational transition	ν (cm^{-1}), our values	$\Delta\nu$ (cm^{-1})
$^4S_{3/2} \leftarrow\leftarrow {}^2P_{3/2}$	79 178.70	573	$F(1; J' = 6) \leftarrow\leftarrow X(0,J'' = 7); P$	79 175.5	3.2
$^2P_{3/2} \leftarrow\leftarrow {}^2P_{3/2}$	79 693.67	1000	$H(0;J' = 2) \leftarrow\leftarrow X(0,J'' = 0); S$	79 686.8	6.8
$^2P_{1/2} \leftarrow\leftarrow {}^2P_{3/2}$	79 867.67	319	$V(m + 8;J' = 6) \leftarrow\leftarrow X(0,J'' = 6);Q$	79 860.5	7.2

analogous findings for other Br-containing compounds.[32] The three strong bromine atomic lines observed in the spectral region discussed here (see above) are all observed in an excitation region corresponding to the low energy tail of the weak *A*-band spectrum where one-photon absorption cross section is very low, of the order 10^{-21} cm^2 molecule^{-1} at room temperature (to be compared with the cross section of about 2.5 $\times$ 10^{-18} cm^2 molecule^{-1} for the maximum of the *A*-band[33]) (see Fig. 1). The two-photon excitation wavenumbers for these lines happen to be very close to HBr molecular resonances (see Fig. 2), the closest of which are listed in Table VI along with details concerning the observed atomic lines. These two-photon absorptions will involve small but nonzero molecular excitations corresponding to the tails of the closest molecular bands. Based on the analysis above all these molecular resonances correspond to excitations to predissociating states which will form bromine atoms. The atom resonance signals will depend on uncertain transition probability parameters, for the molecule and the bromine atom, as well as the density of bromine atoms formed. The relatively largest signal due to the $^2P_{3/2} \leftarrow\leftarrow {}^2P_{3/2}$ atom resonance could be mainly associated with favourable selection rules ($\Delta L = \Delta S = \Delta J = 0$) whereas the significantly larger signal for the $^4S_{3/2} \leftarrow\leftarrow {}^2P_{3/2}$ ($\Delta L = \Delta S = 1$, $\Delta J = 0$) resonance compared to that for the $^2P_{1/2} \leftarrow\leftarrow {}^2P_{3/2}$ ($\Delta L = \Delta S = 0$, $\Delta J = 1$) resonance could be associated with the smaller difference in molecular vs. atom resonances in the former case (Table VI).

CONCLUSIONS

The analyses presented in this paper shine important light on mechanisms of photodissociation processes for H^{i}Br involving Rydberg and ion-pair state interactions. One colour REMPI spectra for atom- and molecular ions of H^{i}Br ($i = 79$, 81) in the two-photon excitation region 79 040–80 300 cm^{-1} have been analysed in terms of rotational line positions, intensities and line-widths. The analyses reveal state interactions of varying strength between Rydberg and ion-pair states. Quantitative analysis of the data relevant to near-resonance interactions between the $F^1\Delta_2(v' = 1)$ and $V^1\Sigma^+(v' = m + 7)$ states give interaction strengths (W_{12}) and fractional state mixing (c_1^2 and c_2^2) as a function of rotational quantum numbers and parameters characteristic for the degree of state mixing (α) and dissociation (γ) of the $F(1)$ state (Table III). Qualitative analysis further reveals the nature of state interactions between the ion-pair states $V(m + k)$ (k = 7,8) and the $E^1\Sigma^+(v' = 1)$ and $H^1\Sigma^+(v' = 0)$ Rydberg states in terms of relative strengths and J' dependences. A great variety in line-widths, hence lifetimes (Table IV), depending on electronic states and J' quantum numbers, is indicative of a number of different predissociation channels. Correlations between those observations and line-shifts and signal intensities reveal dissociation mechanisms involving ion-pair to Rydberg state interactions prior to direct or indirect (via Rydberg gateway states) predissociations of Rydberg states. Major channels are summarized in Fig. 7. The interaction between the $V(m + 7)$ and $F(1)$ states is made possible via heterogeneous coupling(s) of the $F(1)$ state, of which mixing with the $C^1\Pi_1$ state is believed to be important. The $C^1\Pi_1$ state is likely to be a gateway state prior to predissociating by the $t^3\Sigma$ repulsive state, both for the $F(1)$ and the $E(1)$ states. Furthermore, quantum interference effects between states clearly play an important role. Thus lifetimes, of the $E(1)$ state, hence the $V(m + 7)$ state, as well as interactions between these states as a function of J' are found to depend on the interaction between the $V(m + 7)$ and $F(1)$ states. Observed bromine atom (2 + 1) REMPI signals support the importance of Rydberg states predissociation channels. A band system, not previously reported in REMPI, is assigned to the Q branch of the $k^3\Pi_0(v' = 0) \leftarrow\leftarrow X^1\Sigma^+$ transition and analysed to give the band origin 80 038 $\pm$ 2 cm^{-1} and the rotational parameters $B_{v'} = 7.238 \pm 0.070$ cm^{-1} and $D_{v'} = -0.016 \pm 0.005$ cm^{-1} for the k state.

ACKNOWLEDGMENTS

The financial support of the University Research Fund, University of Iceland, the Icelandic Science Foundation as well as the Norwegian Research Council is gratefully acknowledged.

[1] J. H. Seinfeld and S. N. Pandis, *Atmospheric Chemistry and Physics: From Air Pollution to Climate Change* (Wiley, 2006); M. J. Simpson, R. P. Tuckett, K. F. Dunn, C. A. Hunniford, and C. J. Latimer, J. Chem. Phys. **130**, 194302 (2009).
[2] J. I. Lunine, *Astrobiology* (Pearson/Addison-Wesley, 2005); A. M. Shaw, *Astrochemistry: From Astronomy to Astrobiology* (Wiley, 2006).
[3] N. Hoffmann, Chem. Rev. **108**, 1052 (2008).
[4] C. Sandorfy, *The Role of Rydberg states in Spectroscopy and Photochemistry: Low and High Rydberg States* (Kluwer Academic, New York, 2002).
[5] H. Lefebvre-Brion, in *The Role of Rydberg states in Spectroscopy and Photochemistry: Low and High Rydberg States*, edited by C. Sándorfy (Kluwer Academic, New York, 2002), Vol. 20, p. 267.
[6] H. Lefebvre-Brion and R. W. Field, *The Spectra and Dynamics of Diatomic Molecules* (Elsevier, 2004).
[7] A. J. Yencha, D. K. Kela, R. J. Donovan, A. Hopkirk, and Á. Kvaran, Chem. Phys. Lett. **165**, 283 (1990); Á. Kvaran, A. J. Yencha, D. K. Kela, R. J. Donovan, and A. Hopkirk, *ibid.* **179**, 263 (1991); D. Kaur, A. J. Yencha, R. J. Donovan, Á. Kvaran, and A. Hopkirk, Org. Mass Spectrom. **28**, 327 (1993); A. J. Yencha, D. Kaur, R. J. Donovan, Á. Kvaran, A. Hopkirk, H. Lefebvre-Brion, and F. Keller, J. Chem. Phys. **99**, 4986 (1993); K. P. Lawley, A. C. Flexen, R. R. J. Maier, A. Manck, T. Ridley, and R. J. Donovan, Phys. Chem. Chem. Phys. **4**, 1412 (2002); T. Ridley, J. T. Hennessy, R. J.

Donovan, K. P. Lawley, S. Wang, P. Brint, and E. Lane, J. Phys. Chem. A **112**, 7170 (2008).
[8]A. E. Douglas and F. R. Greening, Can. J. Phys. **57**, 1650 (1979).
[9]D. S. Green, G. A. Bickel, and S. C. Wallace, J. Mol. Spectrosc. **150**, 303 (1991); **150**, 354 (1991); **150**, 388 (1991).
[10]R. Callaghan and R. J. Gordon, J. Chem. Phys. **93**, 4624 (1990).
[11]D. Ascenzi, S. Langford, M. Ashfold, and A. Orr-Ewing, Phys. Chem. Chem. Phys. **3**, 29 (2001).
[12]Á. Kvaran, Á. Logadóttir, and H. Wang, J. Chem. Phys. **109**, 5856 (1998).
[13]Á. Kvaran, H. Wang, and Á. Logadóttir, J. Chem. Phys. **112**, 10811 (2000).
[14]R. Liyanage, R. J. Gordon, and R. W. Field, J. Chem. Phys. **109**, 8374 (1998).
[15]Á. Kvaran, B. G. Waage, and H. Wang, J. Chem. Phys. **113**, 1755 (2000); Á. Kvaran, H. Wang, and B. G. Waage, Can. J. Phys. **79**, 197 (2001); Á. Kvaran and H. Wang, J. Mol. Spectrosc. **228**, 143 (2004); S. M. Hurley, Q. Zhong, and J. A. W. Castleman, J. Chem. Phys. **112**, 4644 (2000).
[16]Á. Kvaran and H. Wang, Mol. Phys. **100**, 3513 (2002).
[17]A. I. Chichinin, C. Maul, and K. H. Gericke, J. Chem. Phys. **124**, 224324 (2006); A. I. Chichinin, P. S. Shternin, N. Godecke, S. Kauczok, C. Maul, O. S. Vasyutinskii, and K. H. Gericke, *ibid.* **125**, 034310 (2006); S. Kauczok, C. Maul, A. I. Chichinin, and K. H. Gericke, *ibid.* **133**, 24301 (2010); C. Romanescu and H. P. Loock, *ibid.* **127**, 124304 (2007); C. Romanescu, S. Manzhos, D. Boldovsky, J. Clarke, and H. Loock, *ibid.* **120**, 767 (2004).
[18]C. Romanescu and H. P. Loock, Phys. Chem. Chem. Phys. **8**, 2940 (2006).
[19]Á. Kvaran, H. Wang, K. Matthíasson, A. Bodi, and E. Jonsson, J. Chem. Phys. **129**, 164313 (2008).
[20]A. Kvaran, K. Matthiasson, and H. S. Wang, J. Chem. Phys. **131**, 044324 (2009).
[21]K. Matthiasson, H. S. Wang, and A. Kvaran, J. Mol. Spectrosc. **255**, 1 (2009).
[22]K. Matthíasson, J. M. Long, H. Wang, and Á. Kvaran, J. Chem. Phys. **134**, 164302 (2011).
[23]M. Bettendorff, S. D. Peyerimhoff, and R. J. Buenker, Chem. Phys. **66**, 261 (1982); H. Lefebvre-Brion, H. P. Liebermann, and G. J. Vazquez, J. Chem. Phys. **134** (2011); D. M. Hirst and M. F. Guest, Molecular Physics **41**, 1483 (1980).
[24]J. Long, H. Wang, and A. Kvaran (unpublished).
[25]Á. Kvaran, Ó. F. Sigurbjörnsson, and H. Wang, J. Mol. Struct. **790**, 27 (2006).
[26]D. S. Ginter, M. L. Ginter, and S. G. Tilford, J. Mol. Spectrosc. **90**, 152 (1981).
[27]*NIST Chemistry WebBook* (NIST (National Institute of Standards and Technology) Chemistry WebBook); K. P. Huber and G. Herzberg, *Constants of Diatomic Molecules* (Van Nostrand Reinhold, New York, 1979); online at http://webbook.nist.gov/chemistry/form-ser.html.en-us.en.
[28]G. Herzberg, *Molecular Spectra and Molecular Structure; I. Spectra of Diatomic Molecules*, 2nd ed. (Van Nostrand Reinhold, New York, 1950).
[29]Y. Xie, P. T. A. Reilly, S. Chilukuri, and R. J. Gordon, J. Chem. Phys. **95**, 854 (1991).
[30]A. Kvaran, K. Matthiasson, and H. S. Wang, Chem. Phys. Lett. **458**, 58 (2008).
[31]M. H. Alexander, X. N. Li, R. Liyanage, and R. J. Gordon, Chem. Phys.**231**, 331 (1998).
[32]A. Kvaran, H. S. Wang, K. Matthiasson, and A. Bodi, J. Phys. Chem. A **114**, 9991 (2010); A. Kvaran, K. Sveinbjornsson, J. M. Long, and H. S. Wang, Chem. Phys. Lett. **516**, 12 (2011).
[33]C. E. Brion, A. Dyck, and G. Cooper, J. Electron Spectrosc. Relat. Phenom. **144**, 127 (2005).
[34]A. G. Smolin, O. S. Vasyutinskii, G. G. Balint-Kurti, and A. Brown, J. Phys. Chem. A **110**, 5371 (2006).
[35]J. M. W. Chase, *NIST-JANAF Thermochemical Tables*, 4th ed. (1998), p. 1; online at http://www.nist.gov/pml/data/asd.cfm.